Elastic Boundary Layers in Two-Dimensional Isotropic Lattices

A. Srikantha Phani
Department of Mechanical Engineering,
University of Bath,
Claverton Down,
Bath BA2 7AY, UK
e-mail: spa21@bath.ac.uk

Norman A. Fleck
Department of Engineering,
University of Cambridge,
Trumpington Street,
Cambridge CB2 1PZ, UK
e-mail: naf1@eng.cam.ac.uk

The phenomenon of elastic boundary layers under quasistatic loading is investigated using the Floquet–Bloch formalism for two-dimensional, isotropic, periodic lattices. The elastic boundary layer is a region of localized elastic deformation, confined to the free edge of a lattice. Boundary layer phenomena in three isotropic lattice topologies are investigated: the semiregular Kagome lattice, the regular hexagonal lattice, and the regular fully triangulated lattice. The boundary layer depth is on the order of the strut length for the hexagonal and the fully triangulated lattices. For the Kagome lattice, the depth of boundary layer scales inversely with the relative density. Thus, the boundary layer in a Kagome lattice of low relative density spans many cells.
[DOI: 10.1115/1.2775503]

1 Introduction

Recently, Fleck and Qiu [1] observed elastic boundary layers near the free edge of three isotropic lattices: the regular fully triangulated lattice, the semiregular Kagome lattice, and the regular hexagonal lattice as shown in Fig. 1. They noted that a deep boundary layer exists for the Kagome lattice under remote tension or shear, see Fig. 2. In contrast, the fully triangulated and hexagonal lattices possess boundary layers of depth on the order of one unit-cell size. Fleck and Qiu [1] also calculated the reduction in macroscopic stiffness of a finite-width panel due to the presence of a compliant boundary layer. The drop in stiffness is significant for a Kagome lattice, but not for the fully triangulated and hexagonal lattices.

The boundary layer along the sides of the Kagome lattice provides insight into a paradox in the literature on the effective modulus of triaxial composites. Kueh et al. [2] measured the modulus of carbon-fiber, epoxy-matrix composites with a Kagome weave. They found that the elastic modulus is neither isotropic nor independent of the width of the specimen. Narrow specimens loaded in the direction shown in Fig. 2(*a*) have a lower modulus than wide specimens, while no such width effect was observed for specimens loaded in the transverse direction. These observations are readily explained in terms of the compliant boundary layer as shown in Fig. 2(*a*).

The boundary layer phenomenon can be considered to be an analog of St. Venant's edge solutions in the theory of linear elasticity [3]. The boundary layer can also be thought of as an exponentially decaying wave of zero frequency into the medium from the free edge. Thus, a wave propagation technique can be employed to search for these solutions. The Floquet–Bloch technique has already been employed by the authors [4] in order to compute the band structure of lattice materials. In the present study, this formalism is modified to investigate the phenomenon of elastic boundary layers. The waves of interest are of zero frequency and infinite wavelength along the edge. In this study, a general formulation is developed to search for waves of finite frequency and finite wavelength in the x_2 direction, and an exponentially decaying amplitude, with possible oscillation, in the orthogonal x_1 direction, as defined in Fig. 1. This formalism is then specialized to the quasistatic problem of zero frequency and infinite wavelength along the edge of the lattice. In this limit, the elastic boundary layers shown, for example, in Fig. 2 are the eigensolutions of a quadratic eigenvalue problem (QEP). The eigenvalues give the spatial decay rate of the boundary layer deformation.

The paper is organized as follows. Section 2 gives the formulation of the eigenvalue problem for plane wave propagation at finite frequencies and finite wavelength within a spatially periodic lattice. In Sec. 3, this formalism is used to investigate elastic boundary layers in the three isotropic lattices and the dependence of boundary layer thickness on relative density is computed for the three microstructures. Concluding remarks are given in Sec. 4.

2 Formulation of the Harmonic Wave Propagation Problem

Recall from classical wave theory [5] that a plane wave of frequency ω is represented by the displacement $\mathbf{u}(\mathbf{x},t)$ of a material point $\mathbf{x}$ at time t as

$$\mathbf{u}(\mathbf{x},t) = \mathbf{u}_0 \exp[i(\omega t - \mathbf{k} \cdot \mathbf{x})] \tag{1}$$

where $\mathbf{u}_0$ is the wave amplitude and $\mathbf{k}$ is the wave vector. In this section, we consider the problem of finding all possible plane waves which propagate along the free edge of a lattice and decay into the medium. With reference to the coordinate system already introduced in Fig. 1, assume that surface waves with a finite frequency ω travel along the x_2 direction, and decay, with oscillation, in the orthogonal x_1 direction. For this wave, the wave vector $\mathbf{k}$ has a purely real component k_2 along the x_2 direction and a complex component k_1, with negative imaginary part, along the x_1 direction.

Consider a notional unit cell of any two-dimensional lattice as sketched in Fig. 3. The Cartesian reference frame $(\mathbf{x}_1, \mathbf{x}_2)$ is again employed and the unit base-vector pair $(\mathbf{e}_1, \mathbf{e}_2)$ is introduced. The Euler–Lagrange equations of motion of the unit cell of a spatially periodic lattice panel can be written in the form [4]

$$\mathbf{M}\ddot{\mathbf{q}} + \mathbf{K}\mathbf{q} = \mathbf{f} \tag{2}$$

where $\mathbf{M}$ and $\mathbf{K}$ are the assembled mass and stiffness matrices of the unit cell obtained by following the usual finite element procedure [6]. The vectors $\mathbf{q}$ and $\mathbf{f}$ denote the displacement degrees of freedom and nodal forces of the unit cell, respectively. Here, the unit cell is discretized into a network of Timoshenko beams. Each beam is assumed to have three degrees of freedom at each end: an axial displacement, a transverse displacement, and a rotation of the beam cross section.

Contributed by the Applied Mechanics Division of ASME for publication in the JOURNAL OF APPLIED MECHANICS. Manuscript received February 21, 2007; final manuscript received June 15, 2007; published online February 27, 2008. Review conducted by Robert M. McMeeking.

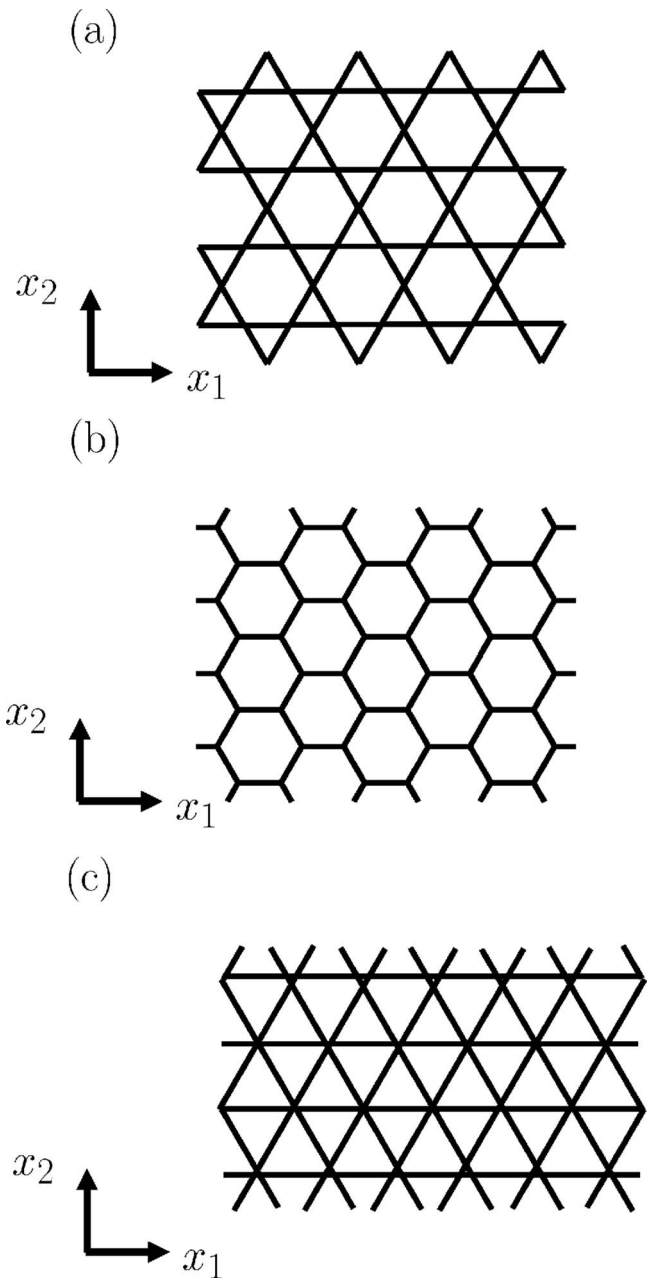

Fig. 1 The two-dimensional isotropic lattices considered in the present study: (*a*) semiregular Kagome lattice, (*b*) regular hexagonal lattice, and (*c*) regular fully triangulated lattice

Assume a time-harmonic displacement solution of the form $\mathbf{q} = \mathbf{q}e^{i\omega t}$. Then Eq. (2) can be simplified to

$$\mathbf{Dq} = \mathbf{f} \quad \text{where } \mathbf{D} \equiv [-\omega^2\mathbf{M} + \mathbf{K}] \tag{3}$$

D is the *dynamic* stiffness and, in the limit of zero frequency, it reduces to the static stiffness matrix **K**. It proves convenient to partition the degrees of freedom of the unit cell into distinct groups, as labeled in Fig. 3. For example, $\mathbf{q}_l$ are the generalized displacements of the nodes on the left-hand side of the unit cell. Similarly, $\mathbf{q}_r$, $\mathbf{q}_b$, $\mathbf{q}_t$, and $\mathbf{q}_i$ refer to the displacements of the nodes situated on the right-hand side, bottom, top, and interior, respectively. The equations of motion given in Eq. (3) can now be written in the partitioned form:

$$\begin{bmatrix} \mathbf{D}_{ll} & \mathbf{D}_{lr} & \mathbf{D}_{lb} & \mathbf{D}_{lt} & \mathbf{D}_{li} \\ \mathbf{D}_{rl} & \mathbf{D}_{rr} & \mathbf{D}_{rb} & \mathbf{D}_{rt} & \mathbf{D}_{ri} \\ \mathbf{D}_{bl} & \mathbf{D}_{br} & \mathbf{D}_{bb} & \mathbf{D}_{bt} & \mathbf{D}_{bi} \\ \mathbf{D}_{tl} & \mathbf{D}_{tr} & \mathbf{D}_{tb} & \mathbf{D}_{tt} & \mathbf{D}_{ti} \\ \mathbf{D}_{il} & \mathbf{D}_{ir} & \mathbf{D}_{ib} & \mathbf{D}_{it} & \mathbf{D}_{ii} \end{bmatrix} \begin{bmatrix} \mathbf{q}_l \\ \mathbf{q}_r \\ \mathbf{q}_b \\ \mathbf{q}_t \\ \mathbf{q}_i \end{bmatrix} = \begin{bmatrix} \mathbf{f}_l \\ \mathbf{f}_r \\ \mathbf{f}_b \\ \mathbf{f}_t \\ \mathbf{f}_i \end{bmatrix} \tag{4}$$

Let $q(\mathbf{r}_j)$ denote the displacement of a lattice point j located by the position vector $\mathbf{r}_j$ in the reference unit cell. If a plane wave solution is admitted, then it follows from Eq. (1) that $q(\mathbf{r}_j)$ is of the form

$$q(\mathbf{r}_j) = q_j \exp i(\omega t - i\mathbf{k} \cdot \mathbf{r}_j) \tag{5}$$

where q_j is the amplitude, ω is the circular frequency, and **k** is the wave vector of the plane wave. With reference to the chosen unit cell, let the integer pair (n_1, n_2) identify any other cell obtained by n_1 translations along the $\mathbf{x}_1$ direction and n_2 translations along the $\mathbf{x}_2$ direction. Then, the position vector of the point within the cell (n_1, n_2), corresponding to the $\mathbf{r}_j$ point in the reference unit cell, is given by

$$\mathbf{r} = \mathbf{r}_j + n_1 l_1 \mathbf{e}_1 + n_2 l_2 \mathbf{e}_2 \tag{6}$$

Substitution of Eq. (6) into Eq. (5) gives

$$q(\mathbf{r}) = q(\mathbf{r}_j) e^{-i\mathbf{k}\cdot(\mathbf{r}-\mathbf{r}_j)} = q(\mathbf{r}_j) e^{-i(k_1 n_1 l_1 + k_2 n_2 l_2)} \tag{7}$$

where l_1 and l_2 are the dimensions of the unit cell of the lattice. This is Bloch's theorem [7–9]. The components (k_1, k_2) of the wave vector **k** are expressed in the general form

$$k_1 \equiv \epsilon_1 + i\delta_1 \quad k_2 \equiv \epsilon_2 + i\delta_2 \tag{8}$$

The real part ϵ and the imaginary part δ of the wave components are called the *phase* and *attenuation* constants, respectively. The phase constant is a measure of the phase change, while the imaginary part is a measure of attenuation of the wave as it travels from one unit cell to the next. The waves of interest in the present study propagate along the x_2 direction and exhibit an exponential decay in the x_1 direction. Consequently, the wave-vector components are given by $k_2 = \epsilon_2, k_1 = \epsilon_1 + i\delta_1$, and $\delta_1 < 0$.

The Bloch wave assumption in the x_1 direction provides connections between nodal quantities on the right and left sides of the unit cell:

$$\mathbf{q}_r = \gamma \mathbf{q}_l \tag{9}$$

$$\mathbf{f}_r = -\gamma \mathbf{f}_l \tag{10}$$

where

$$\gamma \equiv \exp(-ik_1 l_1) \tag{11}$$

The aim is *to find all possible values of the complex quantity* γ *for any specified value of the pair* (ω, k_2). We make further use of Bloch's theorem and equilibrium considerations in the x_2 direction in order to obtain a QEP in γ.

Bloch's theorem and the compatibility of displacements in the x_2 direction enforces the following relationship between the displacements of the shared degrees of freedom along the top-bottom interface of two neighboring cells:

$$\mathbf{q}_t = e^{-ik_2 l_2} \mathbf{q}_b \tag{12}$$

Force equilibrium along the edge at the top-bottom interface requires

$$\mathbf{f}_t + e^{-ik_2 l_2} \mathbf{f}_b = \mathbf{0} \tag{13}$$

while equilibrium of the internal nodes implies

$$\mathbf{f}_i = \mathbf{0} \tag{14}$$

Substitution of the expression for $\mathbf{f}_i$ from Eq. (4) into the above equation gives

$$\mathbf{q}_i = -\mathbf{D}_{ii}^{-1}[\mathbf{D}_{il}\mathbf{q}_l + \mathbf{D}_{ir}\mathbf{q}_r + \mathbf{D}_{ib}\mathbf{q}_b + \mathbf{D}_{it}\mathbf{q}_t] \tag{15}$$

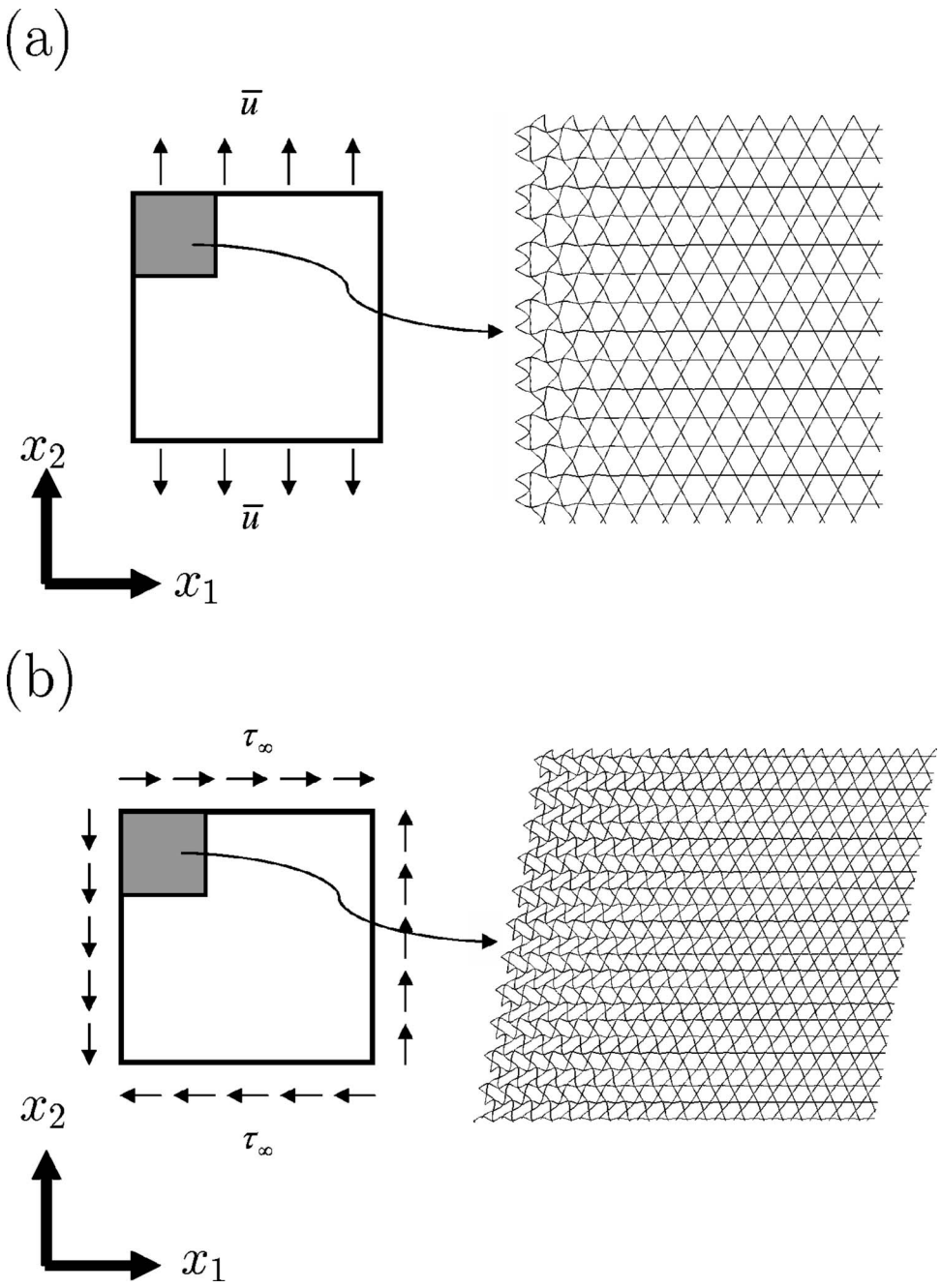

Fig. 2 Deformed mesh of Kagome lattice ($\bar{\rho}$=10%) revealing a boundary layer at the sides of the specimen for (*a*) uniaxial tension and (*b*) simple shear. Based on the work of Fleck and Qiu [1].

Now substitute the expressions for $\mathbf{f}_b$ and $\mathbf{f}_t$ from the third and fourth rows of Eq. (4) into Eq. (13) and use Eqs. (15) and (12) to simplify

$$\mathbf{P}\mathbf{q}_l + \mathbf{Q}\mathbf{q}_r + \mathbf{R}\mathbf{q}_b = \mathbf{0} \tag{16}$$

where the matrices $\mathbf{P}$, $\mathbf{Q}$, and $\mathbf{R}$ are defined as

$$\mathbf{P} \equiv \mathbf{D}_{tl} + \exp(-ik_2l_2)\mathbf{D}_{bl} - \mathbf{D}_{ti}\mathbf{D}_{ii}^{-1}\mathbf{D}_{il} - \exp(-ik_2l_2)\mathbf{D}_{bi}\mathbf{D}_{ii}^{-1}\mathbf{D}_{il}$$

$$\mathbf{Q} \equiv \mathbf{D}_{tr} + \exp(-ik_2l_2)\mathbf{D}_{br} - \mathbf{D}_{ti}\mathbf{D}_{ii}^{-1}\mathbf{D}_{ir} - \exp(-ik_2l_2)\mathbf{D}_{bi}\mathbf{D}_{ii}^{-1}\mathbf{D}_{ir}$$

$$\begin{aligned}\mathbf{R} \equiv [&\mathbf{D}_{tb} + \exp(-ik_2l_2)\mathbf{D}_{bb} - \mathbf{D}_{ti}\mathbf{D}_{ii}^{-1}\mathbf{D}_{ib} - \exp(-ik_2l_2)\mathbf{D}_{bi}\mathbf{D}_{ii}^{-1}\mathbf{D}_{ib}] \\ &+ \exp(-ik_2l_2)[\mathbf{D}_{tt} + \exp(-ik_2l_2)\mathbf{D}_{bt} - \mathbf{D}_{ti}\mathbf{D}_{ii}^{-1}\mathbf{D}_{it} - \exp(\\ &- ik_2l_2)\mathbf{D}_{bi}\mathbf{D}_{ii}^{-1}\mathbf{D}_{it}]\end{aligned} \tag{17}$$

Equation (16) gives the displacement degrees of freedom associated with the bottom nodes $\mathbf{q}_b$ in terms of $\mathbf{q}_l$ and $\mathbf{q}_r$:

$$\mathbf{q}_b = -\mathbf{R}^{-1}[\mathbf{P}\mathbf{q}_l + \mathbf{Q}\mathbf{q}_r] \tag{18}$$

The nodal displacements ($\mathbf{q}_r$, $\mathbf{q}_b$, $\mathbf{q}_t$, $\mathbf{q}_i$) can now be written in terms of $\mathbf{q}_l$ upon using Eqs. (9), (12), (15), and (18). Similarly, the

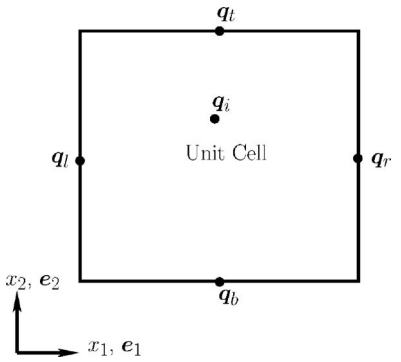

Fig. 3 A unit cell for a two-dimensional periodic structure showing the degrees of freedom shared with the neighboring unit cells and the coordinate system employed

nodal forces ($\mathbf{f}_l$, $\mathbf{f}_r$) can be written in terms of $\mathbf{q}_l$ via the first two rows of Eq. (4). Now enforce the Bloch wave statement in Eq. (10) to obtain a QEP in γ,

$$[\gamma^2\mathbf{A} + \gamma\mathbf{B} + \mathbf{C}]\mathbf{q}_l = \mathbf{0} \tag{19}$$

The matrices **A**, **B**, and **C** are defined as

$$\mathbf{A} \equiv \mathbf{D}_{lr} + \mathbf{D}_{lb}\mathbf{Y} + \exp(-ik_2l_2)\mathbf{D}_{lt}\mathbf{Y} - \mathbf{D}_{li}\mathbf{D}_{ii}^{-1}\mathbf{D}_{ir} - \mathbf{D}_{li}\mathbf{D}_{ii}^{-1}\mathbf{D}_{ib}\mathbf{Y} - \exp(-ik_2l_2)\mathbf{D}_{li}\mathbf{D}_{ii}^{-1}\mathbf{D}_{it}\mathbf{Y}$$

$$\mathbf{B} \equiv \mathbf{D}_{ll} + \mathbf{D}_{lb}\mathbf{X} + \mathbf{D}_{lt}\mathbf{X} - \mathbf{D}_{li}\mathbf{D}_{ii}^{-1}\mathbf{D}_{il} - \mathbf{D}_{li}\mathbf{D}_{ii}^{-1}\mathbf{D}_{ib}\mathbf{X} - \exp(-ik_2l_2)\mathbf{D}_{li}\mathbf{D}_{ii}^{-1}\mathbf{D}_{it}\mathbf{X} + \mathbf{D}_{rr} + \mathbf{D}_{rb}\mathbf{Y} + \exp(-ik_2l_2)\mathbf{D}_{rt}\mathbf{Y} - \mathbf{D}_{ri}\mathbf{D}_{ii}^{-1}\mathbf{D}_{ir} - \mathbf{D}_{ri}\mathbf{D}_{ii}^{-1}\mathbf{D}_{ib}\mathbf{Y} - \exp(-ik_2l_2)\mathbf{D}_{ri}\mathbf{D}_{ii}^{-1}\mathbf{D}_{it}\mathbf{Y} \tag{20}$$

$$\mathbf{C} \equiv \mathbf{D}_{rl} + \mathbf{D}_{rb}\mathbf{X} + \exp(-ik_2l_2)\mathbf{D}_{rt}\mathbf{X} - \mathbf{D}_{ri}\mathbf{D}_{ii}^{-1}\mathbf{D}_{il} - \mathbf{D}_{ri}\mathbf{D}_{ii}^{-1}\mathbf{D}_{ib}\mathbf{X} - \exp(-ik_2l_2)\mathbf{D}_{li}\mathbf{D}_{ii}^{-1}\mathbf{D}_{it}\mathbf{X}$$

where the matrices **X** and **Y** are

$$\mathbf{X} \equiv -\mathbf{R}^{-1}\mathbf{P}$$

$$\mathbf{Y} \equiv -\exp(-ik_2)\mathbf{R}^{-1}\mathbf{Q} \tag{21}$$

The number of eigenvalues is given by twice the dimension N of the displacement vector $\mathbf{q}_l$. The eigenvalues appear as reciprocal complex pairs. For our present purposes of elastic boundary layer analysis, only the exponentially decaying waves are relevant, such that $|\gamma| < 1$. We further limit our attention to the quasistatic eigenstates such that $\omega \equiv 0$ and further specialize the problem to the case where $k_2 \equiv 0$, i.e., there is no variation in the elastic deformation from one unit cell to the other along the x_2 direction.

The joint forces $\tilde{\mathbf{F}}_\mathbf{i}$, $i=1,\ldots,N$, associated with each eigenvector are calculated from Eq. (3) for each eigenvector. Note that the N eigenforce vectors are linearly independent since all eigenvalues are nonzero in Eq. (19). A subset of these eigenstates will be matched with particular solutions for a uniform stress state in the lattice in order to generate the boundary layer solutions.

3 Elastic Boundary Layers in the Quasistatic Case

Consider the three topologies shown in Fig. 1. Boundary layers are now obtained for two separate loading cases. For *loading case 1*, consider a lattice subjected to uniaxial stretching in the x_2 direction while the edge of the lattice is traction free (see Fig. 2(*a*)). For *loading case 2*, consider a lattice subjected to simple shear (see Fig. 2(*b*)). The unit cells employed are shown in Fig. 4.

In general, the stress state of internal bars is not sustainable at the free surface due to the reduced connectivity at the surface. By St. Venant's principle, an elastic boundary layer develops near the free edge. This boundary layer provides a smooth transition of stress state from zero traction at the free edge to a uniform stress state within the lattice. The stress state deep in the interior of the lattice can be obtained by considering the equilibrium of a unit cell under the prescribed external macroscopic loading and using the Cauchy–Born hypothesis [10,11]. Denote this uniform solution, valid in the interior of the lattice, as a particular solution. A complementary function is required such that the sum of the complementary and particular solutions match the free surface boundary conditions on the edge, i. e., the generalized force is zero at the joints lying on the free edge. We shall compute the characteristic solutions which constitute the complementary function needed for a given loading condition by adopting the following procedure.

1. Select the unit cell of a lattice and assemble the dynamic stiffness matrix **D** by following standard finite element procedures.

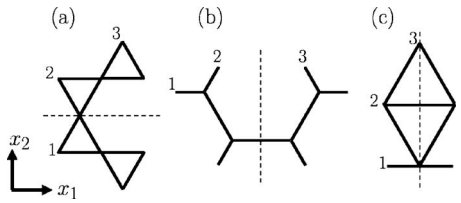

Fig. 4 Unit cells for (*a*) semiregular Kagome lattice, (*b*) regular hexagonal lattice, and (*c*) fully triangulated lattice. The axis of reflective symmetry is shown as a dashed line. Joints on the boundary are labeled numerically.

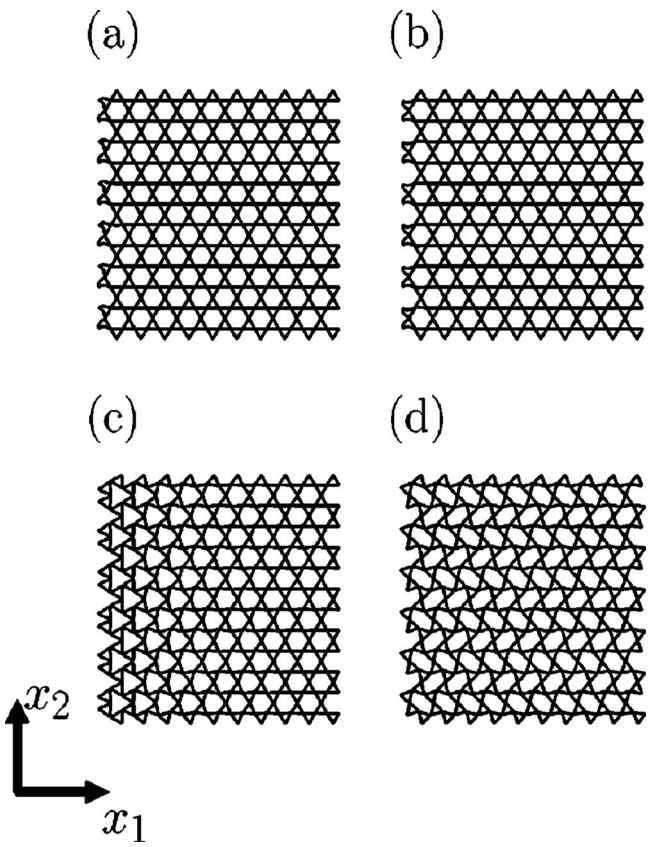

Fig. 5 Boundary layers in a Kagome lattice parallel to the x_2 direction for $\bar{\rho}=0.05$: (*a*) eigenvector 1, (*b*) eigenvector 2, (*c*) eigenvector 3, and (*d*) eigenvector 4

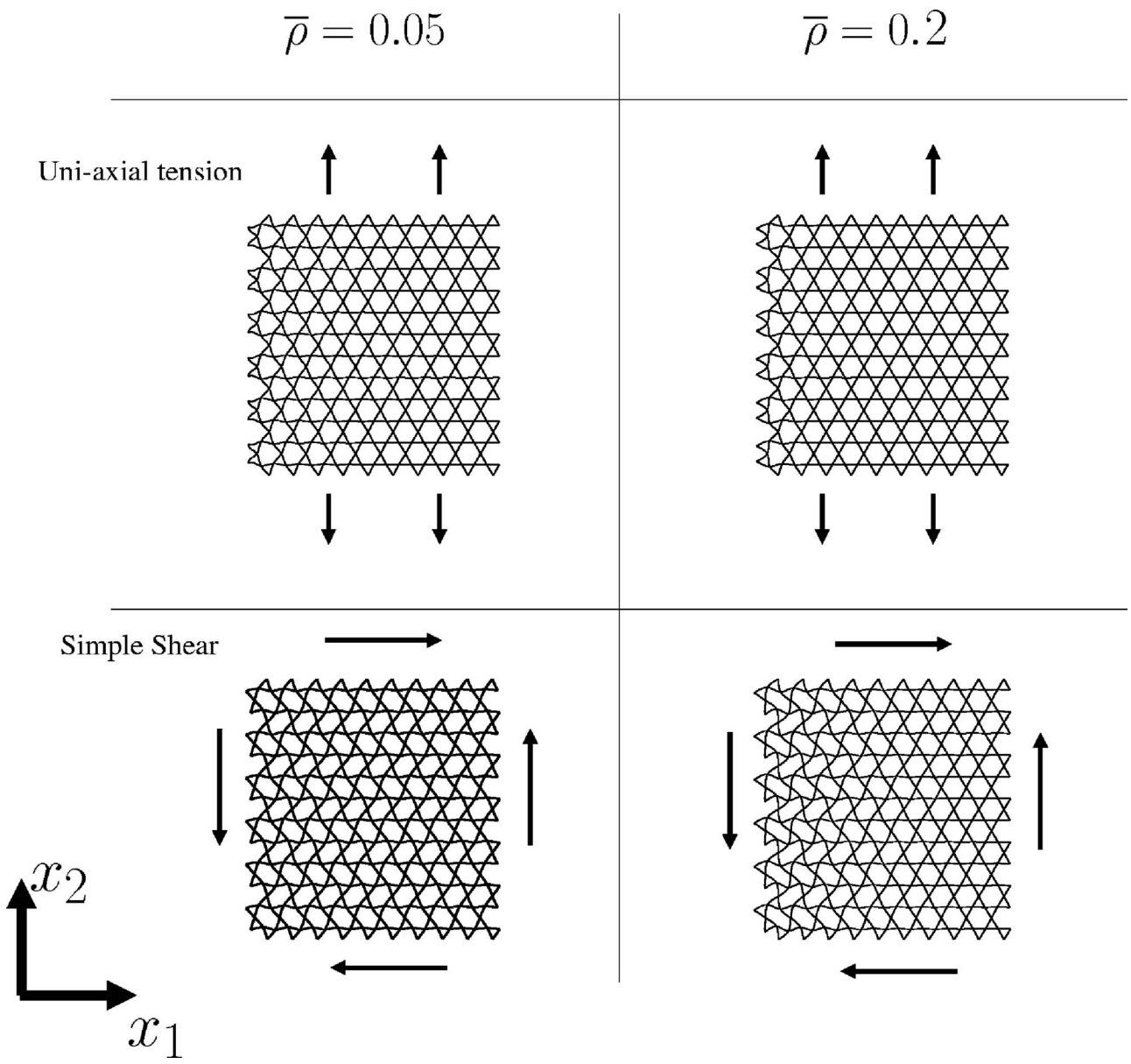

Fig. 6 Elastic boundary layers in a Kagome lattice subjected to macroscopic uniaxial tension along the x_2 direction and subjected to simple shear

2. Specify the pair ($\omega=0$, $k_2=0$) and form the matrices **A**, **B**, and **C** in the eigenvalue problem in Eq. (19).
3. Identify the subset of waves for which the eigenvalue has the property ($|\gamma|=|e^{(-ik_1l_1)}|<1$) as the characteristic waves that constitute the complementary function.
4. Calculate the contribution of each eigenvector to the complementary function by matching with the *known* particular solution, thus completing the solution of the boundary value problem.

We adopt the above procedure in order to construct boundary layer solutions for quasistatic loading of each lattice in turn.

3.1 Kagome Lattice

3.1.1 Boundary Layers Parallel to the x_2 Direction. Consider a Kagome lattice of relative density $\bar{\rho}$ subjected to macroscopic uniaxial stretching in the x_2 direction, as shown in Fig. 2(*a*). The unit cell has six boundary displacement degrees of freedom, $\mathbf{q}_l \in R^6$. The particular solution represents the uniform state of stress within the lattice. This is matched by a suitably chosen complementary function in order for the complete solution to satisfy the free edge boundary conditions. There are two joints, labeled 1 and 2, lying on the free edge for the choice of the unit cell shown in Fig. 4(*a*). Two bars meet at each joint. Three traction-free boundary conditions are specified on each joint in order to satisfy the free-edge boundary condition. Thus, the following six boundary conditions must be satisfied on the free edge:

$$\sum_{b=1}^{2} M_b^j = 0 \quad \sum_{b=1}^{2} V_b^j = 0 \quad \sum_{b=1}^{2} T_b^j = 0 \quad j = 1,2 \tag{22}$$

where M_b^j, V_b^j, and T_b^j denote the bending moment, shear force, and axial force, respectively, exerted by the bar b on the joint j.

Numerical calculations for a Kagome lattice in the quasistatic limit ($\omega=0$, $k_2=0$) show that there are six eigenvector solutions of the eigenvalue problem in Eq. (19): Two of these eigenvectors are the rigid-body displacements ($|\gamma|=1$), consistent with the earlier study of the present authors in Ref. [4]. The remaining four waves

comprise exponentially attenuating waves in the x_1 direction so that the eigenvalue of Eq. (19) satisfies the property $|\gamma|<1$. The four attenuating waves are shown in Fig. 5 for the relative density $\bar{\rho}$ equal to 0.05. The joint forces associated with each eigenvector $\tilde{\mathbf{F}}_i$, $i=1,\ldots,4$, are calculated via Eq. (3). The relative contribution of each of the four eigenvectors to the complementary function is evaluated as follows.

Let the vector $\mathbf{F}\in R^6$ denote the forces due to the particular solution acting on the two joints 1 and 2 as labeled in Fig. 4(*a*). This vector is obtained by considering the equilibrium of the infinite lattice under prescribed macroscopic loading (see Refs. [10,11] for details). The free-edge conditions in Eq. (22) are matched by finding a complementary force vector $\tilde{\mathbf{F}}\in R^6$ such that

$$\mathbf{F}+\tilde{\mathbf{F}}=\mathbf{0} \tag{23}$$

The complementary solution $\tilde{\mathbf{F}}$ is expressed as a linear superposition of the independent eigenforce vectors associated with each of the exponentially decaying eigenvectors as

$$\tilde{\mathbf{F}}=\sum_{i=1}^{4} a_i\tilde{\mathbf{F}}_i \tag{24}$$

where $|\tilde{\mathbf{F}}_i|$ is normalized to unity for each eigenforce vector. The amplitudes a_i of each of these exponentially decaying eigenvector are obtained from the matching condition in Eq. (23). For definiteness, the amplitudes are scaled such that the maximum value of the set is equal to unity.

The amplitudes of the four attenuating eigenvectors in the case of macroscopic uniaxial tensile loading are $\mathbf{a}=[0,0.7,1,0]$. In the case of macroscopic simple shear loading, the amplitudes are $\mathbf{a}=[0.4,0,0,1]$.

The above results are consistent with the reflective symmetry of the Kagome lattice and loading states. Recall that the unit cell of the Kagome lattice in Fig. 4(*a*) has a horizontal axis of reflective symmetry, as indicated by the dashed line. About this axis of symmetry, the tensile loading is symmetric, while the simple shear loading is antisymmetric. It can be seen from Fig. 5 that the deformation of the unit cell in second and third eigenvectors exhibits reflective symmetry about the horizontal axis, whereas the first and fourth eigenvectors show antisymmetric deformation. Hence, only symmetric eigenvectors contribute to the complementary function in the case of uniaxial tensile loading, whereas only antisymmetric eigenvectors contribute in the case of simple shear loading. The resultant boundary layer in each case is shown in Fig. 6 for two values of relative density equal to 0.05 and 0.2, respectively. It can be seen that the boundary layer is much deeper for the case of lower relative density.

In each loading case, the smallest value of δ_i, $i=1,\ldots,4$, for which $|a_i|>0$ governs the boundary layer thickness. The dependence of the attenuation constant $\lambda\equiv\delta_1 l_1$ on the relative density $\bar{\rho}$ is shown in Fig. 7 for each of the eigenvectors. For waves 1 and 2, λ is approximately equal to 4, independent of $\bar{\rho}$. These waves decay rapidly within one unit cell. In contrast, for waves 3 and 4, λ scales linearly with $\bar{\rho}$, and these waves decay only gradually from one unit cell to the next. Recall that the boundary layer for uniaxial tension involves waves 2 and 3, whereas the boundary layer for shear involves waves 1 and 4. Consequently, the depth of the boundary layers in uniaxial tension and in shear both scale as $1/\bar{\rho}$. We conclude that very deep boundary layers exist for lattices of low relative density. A similar dependence of boundary layer depth on $\bar{\rho}$ was noted previously by Fleck and Qiu in Ref. [1]. The specimen size effect observed in the experimental studies of Kueh et al. [2] can now be explained by the presence of an elastic boundary layer.

3.1.2 Boundary Layers Parallel to the x_1 Direction. Next, consider the case when the Kagome lattice is loaded along the x_1 direction, following the same analysis as that described above. There is now only one joint of the unit cell, labeled 3 in Fig. 4(*a*), that lies on the free edge. Hence, the unit cell has three boundary displacement degrees of freedom, $\mathbf{q}_l\in R^3$. In the quasistatic limit ($\omega=0$, $k_1=0$), we find that there are three eigenvector solutions of the eigenvalue problem in Eq. (19), of which two are rigid-body displacements and one is an exponentially attenuating wave in the x_2 direction for which the eigenvalue of Eq. (19) satisfies the property $|\gamma|<1$.

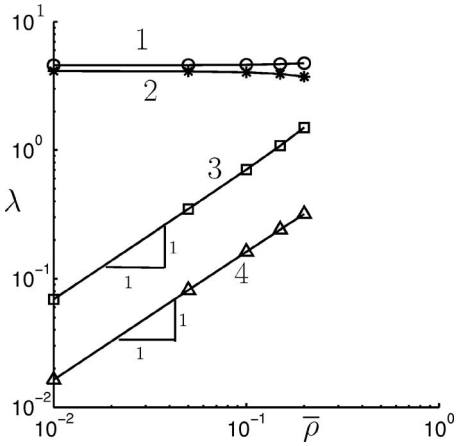

Fig. 7 The attenuation of each of the four eigenvectors versus $\bar{\rho}$ in a Kagome lattice

The eigenvector with the property $|\gamma|<1$ is sketched in Fig. 8. It is characterized by a displacement field $u_2=0$, $u_1>0$ together with joint rotation which decay rapidly with depth x_2. This eigenvector is activated when the top face of a Kagome lattice is subjected to a uniform displacement in the x_1 direction, with unconstrained rotation of the joints.

The above eigenvalue analysis was repeated for selected values of relative density in the range $10^{-2}-10^{-1}$. It was found that λ equals 3.8 in all cases, with a unique eigenvector.

3.2 Hexagonal and Triangular Lattices. An eigenvalue analysis to extract the spatially decaying waves has been performed for a hexagonal lattice and a fully triangulated lattice. The unit cells employed are sketched in Figs. 4(*b*) and 4(*c*). Eigenwaves parallel to the x_1 and x_2 directions are investigated for both lattices for selected values of relative density $\bar{\rho}$ in the range $10^{-2}-10^{-1}$.

Consider first the boundary layer solutions parallel to the x_2 direction in a hexagonal lattice. There is only one joint of the unit cell, labeled 1 in Fig. 4(*b*), that lies on the free edge. Hence $\mathbf{q}_l$

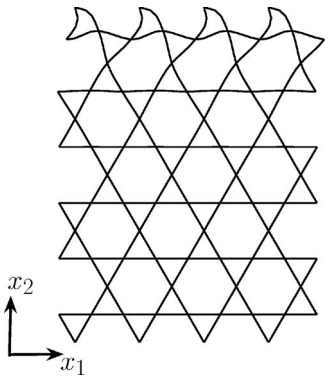

Fig. 8 Boundary layer in a Kagome lattice parallel to the x_1 direction for $\bar{\rho}=0.05$

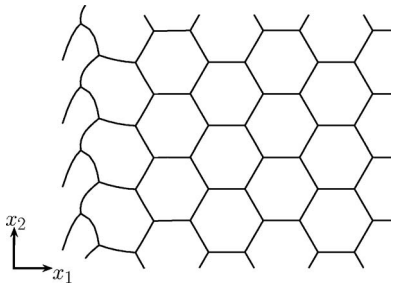

Fig. 9 Boundary layer in a hexagonal lattice parallel to the x_2 direction, for $\bar{\rho}=0.05$

$\in R^3$. In the quasistatic limit ($\omega=0$, $k_2=0$), we find that there are three eigenvector solutions of the eigenvalue problem in Eq. (19), of which two are rigid-body displacements and one is an exponentially attenuating wave in the x_1 direction so that the eigenvalue of Eq. (19) satisfies the property $|\gamma|<1$. The deformation associated with this eigenvector is sketched in Fig. 9. It exhibits a rapid decay of the deformation within one unit cell of the lattice. The eigenvalue analysis was repeated for selected values of relative density in the range $10^{-2}-10^{-1}$. The eigenvector was unchanged and the value of $\lambda \equiv \delta_1 l_1$ equals 5.5 in all cases.

Next, consider the boundary layer solutions parallel to the x_1 direction. There are now two joints of the unit cell, labeled 2 and 3 in Fig. 4(*b*), that lie on the free edge. Hence, the unit cell has six boundary displacement degrees of freedom, $\mathbf{q}_t \in R^6$. In the quasistatic limit ($\omega=0$, $k_1=0$), we find that there are six eigenvector solutions, of which two are rigid-body displacements and four are exponentially attenuating waves in the x_2 direction such that $|\gamma|<1$ in Eq. (19). The elastic deformation corresponding to the four eigenvectors is shown in Fig. 10. Note that the eigenvector deformations in Figs. 10(*a*) and 10(*c*) are symmetric about the vertical

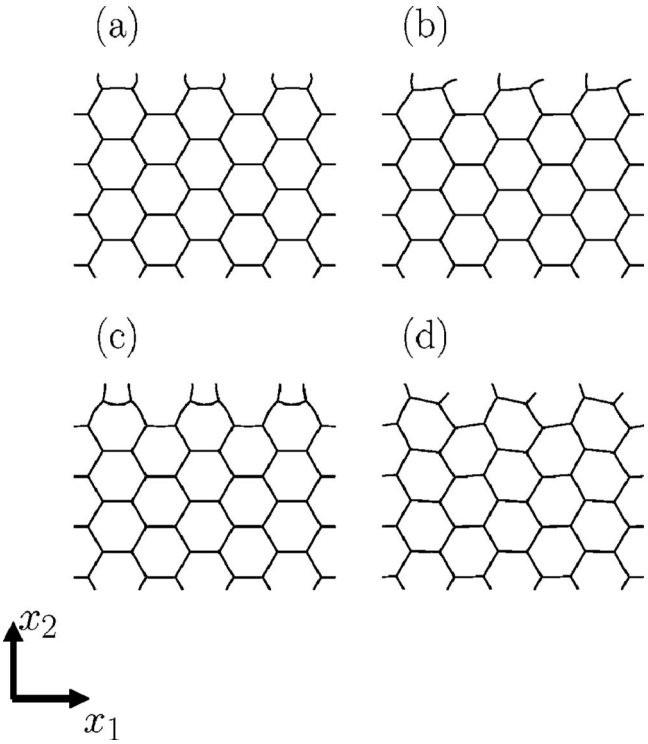

Fig. 10 Boundary layers in a hexagonal lattice parallel to the x_1 direction for $\bar{\rho}=0.05$: (*a*) eigenvector 1, (*b*) eigenvector 2, (*c*) eigenvector 3, and (*d*) eigenvector 4

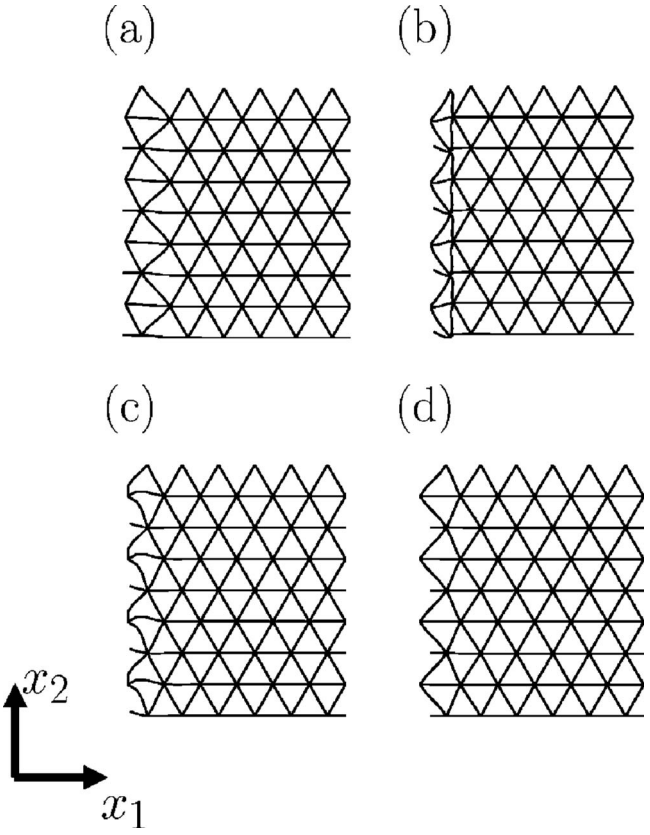

Fig. 11 Boundary layers in a fully triangulated lattice parallel to the x_2 direction for $\bar{\rho}=0.05$: (*a*) eigenvector 1, (*b*) eigenvector 2, (*c*) eigenvector 3, and (*d*) eigenvector 4

axis of reflective symmetry of the unit cell in Fig. 4(*b*), while the eigenvector deformations in Figs. 10(*b*) and 10(*d*) are antisymmetric. The eigenvalue analysis was repeated for selected values of relative density in the range $10^{-2}-10^{-1}$. It was found that $\lambda \equiv \delta_2 l_2$ equals 8.8, 5.3, 3.6, and 1.7 for the four waves shown in Figs. 10(*a*)–10(*d*), respectively. Also, each eigenvector is insensitive to the magnitude of relative density.

A similar analysis has been performed for the triangular lattice to obtain boundary layers parallel to the x_1 and x_2 directions. Consider first a boundary layer parallel to the x_2 direction. The unit cell has six boundary degrees of freedom, $\mathbf{q}_l \in R^6$, since there are two joints on the free edge, labeled 1 and 2 in Fig. 4(*c*). The elastic deformations of the lattice associated with the four exponentially decaying waves in the quasistatic limit ($\omega=0$, $k_2=0$) are sketched in Figs. 11(*a*)–11(*d*). It can be seen that the region of elastic deformation is confined to one unit cell for all eigenvectors. The eigenvalue analysis was repeated for selected values of relative density in the range $10^{-2}-10^{-1}$. The eigenvectors remain unchanged, with $\lambda \equiv \delta_1 l_1$ equal to 9.2, 2.5, 2.4, and 1.4 for the four waves shown in Figs. 11(*a*)–11(*d*), respectively.

Finally, consider possible boundary layer along the x_1 direction. A single eigenvector decays in the x_2 direction, as sketched in Fig. 12. Recall that the unit cell has three boundary degrees of freedom, $\mathbf{q}_t \in R^3$, since there is only one joint on the free edge, labeled 3 in Fig. 4(*c*). The shape of the eigenvector is fixed and $\lambda \equiv \delta_2 l_2$ equals 3.9 for a relative density in the range $10^{-2}-10^{-1}$.

The above study reveals that the boundary layer depth is on the order of the unit-cell size and hence has a negligible influence on the elastic stiffness of a finite-width panel made from a hexagonal lattice or a fully triangulated lattice. These observations are consistent with the earlier study of Fleck and Qiu [1].

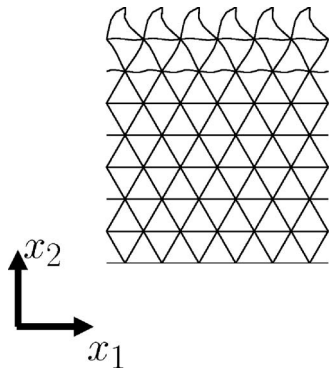

Fig. 12 Boundary layer in a fully triangulated lattice parallel to the x_1 direction for $\bar{\rho}=0.05$.

4 Concluding Remarks

A general formulation based on Floquet-Bloch theory has been developed to compute the elastic boundary layer solutions in two-dimensional periodic lattices. The special case of boundary layers in the quasistatic limit of zero frequency and infinite wavelength along the free edge of the lattice is investigated for three isotropic lattices: a semiregular Kagome lattice, a regular hexagonal lattice, and a fully triangulated lattice.

The Kagome lattice displays deep boundary layers when loaded along particular directions. The analysis presented here provides a theoretical justification for the observation of Fleck and Qiu [1] that the boundary layer depth scales as $1/\bar{\rho}$.

The eigenvector analyses for a hexagonal and a fully triangulated lattice reveal that the characteristic decay length is on the order of the strut length, independent of the relative density. Consequently, elastic boundary layers have negligible influence on the stiffness of the finite specimen made from these lattices.

This study has been restricted to lattices under quasistatic loading. In the general case of finite frequency dynamic loading, it is of practical importance to know if free surface waves of Rayleigh type exist in these periodic media. The formalism developed here can be employed to search for free surface waves in lattices, and this is the subject of a future publication.

References

[1] Fleck, N. A. and Qiu, X., 2007, "The Damage Tolerance of Elastic-Brittle Two Dimensional Isotropic Lattices," J. Mech. Phys. Solids, **55**(3), pp. 562–588.
[2] Kueh, A., Soykasap, O., and Pellegrino, S., 2005, "Thermo-Mechanical Behaviour of Single-ply Triaxial Weave Carbon Fibre Reinforced Plastic," *Proceedings of the European Conference on Spacecraft Structures, Materials and Testing*, Noordwijk, The Netherlands.
[3] Timoshenko, S. P., and Goodier, J. N., 1982, *Theory of Elasticity*, 3rd ed. McGraw-Hill, Singapore.
[4] Srikantha Phani, A., Woodhouse, J., and Fleck, N. A., 2006, "Wave Propagation in Two-Dimensional Periodic Lattices," J. Acoust. Soc. Am., **119**(4), pp. 1995–2005.
[5] Achenbach, J. D., 1973, *Wave Propagation in Elastic Solids*, 2nd ed., North-Holland, New York.
[6] Weaver, W., and Jonhston, P. R., 1987, *Structural Dynamics by Finite Elements*, 1st ed., Prentice-Hall, Englewood Cliffs, NJ.
[7] Brillouin, L., 1953, *Wave Propagation in Periodic Structures*, 2nd ed., Dover, New York.
[8] Kittel, C., 1962, *Elementary Solid State Physics: A Short Course*, 1st ed., Wiley, New York.
[9] Langley, R. S., Bardell, N. S., and Ruivo, H. M., 1997, "The Response of Two-Dimensional Periodic Structures to Harmonic Point Loading: A Theoretical and Experimental Study of a Beam Grillage," J. Sound Vib., **207**(4), pp. 521–535.
[10] Hutchinson, R. G., 2004, "Mechanics of Lattice Materials," Ph.D thesis, University of Cambridge, Cambridge, UK.
[11] Hutchinson, R. G., and Fleck, N. A., 2006, "The Structural Performance of the Periodic Truss," J. Mech. Phys. Solids, **54**, pp. 756–782.